New Journal of Physics
The open access journal at the forefront of physics

Deutsche Physikalische Gesellschaft DPG
IOP Institute of Physics

Published in partnership with: Deutsche Physikalische Gesellschaft and the Institute of Physics

OPEN ACCESS

RECEIVED
19 November 2018

REVISED
4 April 2019

ACCEPTED FOR PUBLICATION
30 May 2019

PUBLISHED
20 June 2019

PAPER

Describing many-body localized systems in thermal environments

Ling-Na Wu[1], **Alexander Schnell**[1], **Giuseppe De Tomasi**[1,2], **Markus Heyl**[1] **and André Eckardt**[1]

[1] Max-Planck-Institut für Physik komplexer Systeme, Nöthnitzer Straße 38, D-01187-Dresden, Germany
[2] Present address: Department of Physics, T42, Technische Universität München, James-Franck-Straße 1, D-85748 Garching, Germany

E-mail: lnwu@pks.mpg.de **and** eckardt@pks.mpg.de

Keywords: many body localization, thermal environment, Lindblad master equation, variable range hopping, quantum-jump Monte Carlo, kinetic theory

Abstract

In this work we formulate an efficient method for the description of fully many-body localized systems in weak contact with thermal environments at temperature T. The key idea is to exploit the representation of the system in terms of quasi-local integrals of motion (l-bits) to efficiently derive the generator for the quantum master equation in Born–Markov approximation. We, moreover, show how to compute the steady state of this equation efficiently by using quantum-jump Monte-Carlo techniques as well as by deriving approximate kinetic equations of motion. As an example, we consider a one-dimensional disordered extended Hubbard model for spinless fermions, for which we derive the l-bit representation approximately by employing a recently proposed method valid in the limit of strong disorder and weak interactions. Coupling the system to a global thermal bath, we study the transport between two leads with different chemical potentials at both of its ends. We find that the temperature-dependent current is captured by an interaction-dependent version of Mott's law for variable range hopping, where transport is enhanced/lowered depending on whether the interactions are attractive or repulsive, respectively. We interpret these results in terms of spatio-energetic correlations between the l-bits.

1. Introduction

Many-body localization (MBL) has emerged as a new paradigm for phase structures in interacting quantum matter protected by the underlying robust nonergodicity imposed by strong disorder [1–6]. This has led to the discovery of novel topological or symmetry-broken phases [4, 7–11], which cannot exist in thermalizing systems, with the particularly prominent example of time crystals breaking not only spatial but also temporal symmetries [12–16]. Although many signatures of MBL have been accessed experimentally [17–24], dissipation induced by a remaining coupling to an environment, even if weak, has turned out to have a crucial impact onto the long-time dynamics [24–33]. Specifically, external baths with large bandwidths and delocalized excitations are expected to force MBL systems towards thermalization, which destabilizes the nonergodic properties central for the anticipated new phase structures. However, it is a challenge to theoretically describe interacting many-body systems coupled to thermal environments for concrete microscopic models.

A standard approach to describe the dynamics of an open system is to use a quantum Lindblad master equation under Born–Markov approximation [34], where the dissipation processes due to the weak coupling to the environment are included in terms of a set of quantum jump operators. For thermal environments, the dissipation is captured by quantum jumps between different eigenstates of the system. Thus, in order to compute the generator of the master equation, it is necessary to fully diagonalize the system. This is challenging for most interacting quantum systems, with the computational effort generally growing exponentially with system size. This difficulty is also reflected in the fact that previous studies are either limited to small system sizes [32, 35–40] or make rather specific assumptions regarding the properties of the environment, e.g. describing it by classical noise [33, 41] or by dephasing processes corresponding to an infinite-temperature thermal environment [27–31, 42].

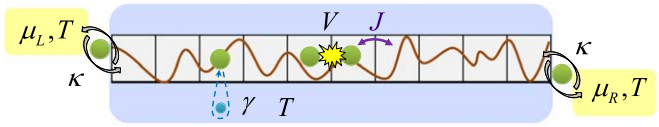

Figure 1. Schematic illustration of the model under consideration. An open tight-binding chain of interacting spinless fermions (green dots) in a random potential (brown curve) is coupled to a global heat bath at temperature T (blue box). This global bath induces phonon (blue dot)-assisted heat exchange with the system and two local baths (yellow boxes) at the ends with different chemical potentials (μ_L and μ_R), which induce particle transport through the chain.

Here we propose to exploit the l-bit representation [43–48] of MBL systems to address the diagonalization problem. The existence of an extensive number of quasi-local integrals of motion in MBL systems makes them special in the sense that they are interacting quantum systems whose full many-body spectrum can be accessed efficiently. While deriving explicitly the l-bit representation is in general a demanding task, the difficulty grows only polynomially with system size [49–52]. Utilizing the l-bit representation, we derive a Lindblad master equation which describes MBL systems weakly coupled to thermal environments. In order to perform concrete calculations, we consider the limit of strong disorder and weak interactions and make use of a recently proposed efficient approximate method [53], where the l-bits are in leading order obtained by a single-particle transformation. Note that a better approximation for the l-bits can be obtained systematically, e.g. by treating the omitted matrix elements perturbatively [28, 50, 51].

Although it is still computationally demanding to solve the full dynamics of the master equation, the steady state of the system in the weak coupling limit can be calculated efficiently. In this case, the steady state is diagonal in the eigenbasis given by the Fock states of the single-particle Hamiltonian under our approximation. Thus it can be obtained through classical Monte-Carlo simulations by mapping the Fock-space occupation probabilities to a classical random walk.

We benchmark our method by studing a spinless fermionic Hubbard chain with strong onsite disorder and weak interactions. The system is coupled to a phonon bath at temperature T. Further, we couple the chain at both ends to fermionic reservoirs with a chemical potential difference. This gives rise to a nonequilibrium current-carrying steady state, which reduces to the conventional linear response regime in the limit of vanishing chemical potential difference. We show how to solve the Lindblad master equation which describes the dynamics of the system by means of classical quantum-jump Monte-Carlo simulations [54]. In order to push our description to even larger systems we use a further simplification of the master equation in terms of a kinetic theory, which shows excellent agreement with the Monte-Carlo simulations for small system sizes, but with the advantage that it allows us to reach system sizes of the order of 100 lattice sites.

Using this formalism, we investigate the transport properties of the nonequilibrium steady state (NESS). We first map out the full temperature dependence of the induced current for the noninteracting problem. At asymptotically low temperatures we observe that the current becomes temperature-independent due to the coherent evolution of particles across the full chain, occurring with an amplitude which is exponentially suppressed as a function of system size. Upon increasing temperature beyond this system-size dependent asymptotic regime, we recover a conductivity following Mott's law for variable-range hopping (VRH), $\sigma \propto \exp[-\sqrt{T_0/T}]$, which is well-studied for Anderson localized systems of noninteracting particles [55]. We take this as a first indication that our approach captures the relevant physics. At even higher temperature, transport crosses over to a simple activated regime where $\sigma \propto \exp[-T_1/T]$. There, particles can overcome typical energy barriers imposed by the strong disorder potential on short distances as opposed to VRH, which is characterized by longer-ranged tunneling processes involving smaller energy changes. We then apply our approach to the weakly interacting case at strong disorder. In the temperature regime where the Anderson system shows VRH, we again find that transport follows Mott's law, in agreement with the analytical prediction of [56]. However, the Mott temperature T_0 is modified by interactions. Depending on whether interactions are repulsive or attractive, T_0 increases or decreases with respect to the noninteracting Anderson insulating case. We interpret the modifications of T_0 in terms of interaction-induced changes in the spatio-energetic correlations among the local integrals of motion in the MBL system.

The paper is organized as follows. In section 2, we present a general scheme to address MBL systems in the presence of thermal baths. We first write out a Lindblad master equation for the l-bits. In the next step, we simplify it further by neglecting the particle-hole dressing which is reasonable in the regime of strong disorder and weak interactions. In section 3, we describe the model (figure 1) which we will study in order to benchmark our approach. This is followed by the introduction of the quantum-jump Monte-Carlo method and the kinetic theory that we utilize to solve the Lindblad master equation in section 4. A good match of the results between these two methods is shown. In section 5, we study the transport properties of the steady state for the

noninteracting system. The discussion for the interacting system is presented in section 6. Finally, a summary of the main results is given in section 7 to conclude.

2. Master equation for many-body localized systems in the presence of thermal baths

When a quantum system is brought into weak contact with a thermal environment, the impact of the environment can be captured by quantum jumps between different eigenstates of the system. The rate at which such a process occurs depends on the energy difference of the corresponding states. For most interacting quantum systems, however, the full spectrum is hard to obtain, so already deriving the equations of motion of the system in the presence of a thermal environment is challenging. We approach this problem by exploiting the fact that MBL systems posses an extensive number of integrals of motion [43–46]. This makes them very special in the sense that they are interacting quantum systems whose full many-body spectrum can be accessed. We make use of this fact to find equations of motion for MBL systems in thermal environments.

2.1. Born–Markov master equation

We are interested in the typical setup of open quantum systems described by the total Hamiltonian

$$\hat{H}_{\rm tot} = \hat{H} + \hat{H}_{\rm SB} + \hat{H}_{\rm B}. \tag{1}$$

Here, $\hat{H}$ denotes the Hamiltonian of the system under investigation, $\hat{H}_{\rm B} = \sum_\alpha \hbar\omega_\alpha \hat{b}_\alpha^\dagger \hat{b}_\alpha$ describes the bath with bosonic or fermionic annihilation operator $\hat{b}_\alpha$ for the mode with energy $\hbar\omega_\alpha$, and $\hat{H}_{\rm SB}$ is the system-bath coupling operator, whose overall strength γ we assume to be small. The bath is assumed to be in thermal equilibrium with temperature T and chemical potential μ.

In the weak-coupling limit ($\gamma \to 0$) and assuming large thermal baths, the dynamics of the reduced density matrix $\hat{\rho} = {\rm Tr}_{\rm B}\{\hat{\rho}_{\rm tot}\}$ of the system after tracing out the bath, can be described using the Born–Markov and the rotating wave approximation. This gives rise to a Lindblad master equation [34]

$$\partial_t \hat{\rho} = -\frac{\rm i}{\hbar}[\hat{H},\, \hat{\rho}] + \sum_\alpha \left(\hat{L}_\alpha \hat{\rho} \hat{L}_\alpha^\dagger - \frac{1}{2}\{\hat{L}_\alpha^\dagger \hat{L}_\alpha,\, \hat{\rho}\} \right) \equiv -\frac{\rm i}{\hbar}[\hat{H},\, \hat{\rho}] + \mathcal{D}(\hat{\rho}), \tag{2}$$

where $\{\,\cdot\,,\cdot\,\}$ denotes the anti-commutator. The first term describes the unitary evolution, and the second term describes the coupling of the system to the environment. Here the operators $\hat{L}_\alpha$ describe quantum jumps between the eigenstates of the system.

Let us assume a system with spectrum E_k and eigenstates $|k\rangle$ coupled to a phonon bath with bosonic operators $\hat{b}_\alpha$ via the system operator $\hat{v}$

$$\hat{H}_{\rm SB} = \gamma \hat{v} \otimes \sum_\alpha \lambda_\alpha (\hat{b}_\alpha + \hat{b}_\alpha^\dagger). \tag{3}$$

Then, the master equation takes the form

$$\partial_t \hat{\rho} = -\frac{\rm i}{\hbar}[\hat{H},\, \hat{\rho}] + \sum_{k,q} \left(\hat{L}_{kq} \hat{\rho} \hat{L}_{kq}^\dagger - \frac{1}{2}\{\hat{L}_{kq}^\dagger \hat{L}_{kq},\, \hat{\rho}\} \right). \tag{4}$$

The bath induces quantum jumps from level q to k, mediated by the action of the jump operators

$$\hat{L}_{kq} = \sqrt{R_{kq}}\, |k\rangle\langle q|, \tag{5}$$

with the jump rates

$$R_{kq} = \frac{2\pi\gamma^2}{\hbar} |\langle k|\hat{v}|q\rangle|^2 g(E_k - E_q). \tag{6}$$

Here we have defined the bath correlation function

$$g(E) = \begin{cases} J(E) n_{\rm B}(E,\, T) & \text{for } E \geqslant 0 \\ J(-E)[1 + n_{\rm B}(-E,\, T)] & \text{for } E < 0 \end{cases} \tag{7}$$

with the Bose distribution $n_{\rm B}(E,\, T) = (e^{E/k_{\rm B}T} - 1)^{-1}$ and the spectral density of the bath $J(E) = \sum_\alpha \lambda_\alpha^2 \delta(E - \hbar\omega_\alpha)$. Note that the Born–Markov and rotating-wave approximations rely on the assumption of a separation of timescales [34]. For them to be valid, the time scales of the system dynamics, $|E_k - E_q|^{-1}$ need to be fast when compared to the bath relaxation time and to the associated time-scales of the system-bath coupling R_{kq}^{-1} (we set $\hbar = k_{\rm B} = 1$ hereafter), respectively[3].

[3] The situation, where these conditions are not fulfilled, was discussed, for instance in [57, 58].

Under the dynamics of equation (4), the coherences, $\langle k|\hat{\rho}|q\rangle$ with $k \neq q$, decay such that the steady state reached asymptotically in the long-time limit is diagonal in the energy basis, $\hat{\rho} \to \hat{\rho}_\infty = \sum_k p_k |k\rangle\langle k|$ [59–61]. This can be seen most easily by noting that in the limit $\gamma \to 0$, the first term in equation (2) has to vanish for the steady state with $\partial_t \hat{\rho}_\infty = 0$. After a diagonal state is reached, the asymptotic dynamics is governed by dissipative processes only and described by the Pauli rate equation

$$\partial_t p_k = \sum_q (R_{kq} p_q - R_{qk} p_k). \tag{8}$$

When the system is coupled to a single bath of temperature T, the rates obey the equilibrium condition $R_{kq}/R_{qk} = \mathrm{e}^{-(E_k - E_q)/T}$. In this case the system approaches thermal equilibrium in the long-time limit, $p_k \propto \exp(-E_k/T)$, and the system obeys detailed balance: the terms of the sum in equation (8), which correspond to the net probability currents from states q to k, vanish individually. If the equilibrium condition is broken, e.g. when the system is coupled to baths of different temperature or chemical potential, the system approaches a non-equilibrium steady state, for which the right-hand side of equation (8) vanishes only as a whole, so that probability currents break detailed balance.

2.2. Many-body localized systems

Note that in order to find the equations of motion for the system in the presence of a thermal bath, it is essential to diagonalize the full Hamiltonian to find its eigenstates and eigenenergies. For a quantum many-body system, this is generally difficult. Non-interacting systems however can be treated readily [62, 63], since the many-body eigenstates are given by the Fock states of the single-particle Hamiltonian. As we discuss in the following, MBL systems provide another exception, due to an emergent form of integrability [43–46].

We consider a system of spinless lattice fermions. A typical example for such a fermionic system with an MBL phase is the one-dimensional Anderson model of spinless fermions with nearest-neighbor interactions V, which we introduce in section 3. The generalization to spinful fermions or spin Hamiltonians is straightforward. We assume that the system Hamiltonian can be brought into the diagonal form

$$\hat{H} = \sum_k \varepsilon_k \hat{n}_k + \frac{1}{2}\sum_{k,q} U_{kq} \hat{n}_k \hat{n}_q + \frac{1}{6}\sum_{k,q,p} U_{kqp} \hat{n}_k \hat{n}_q \hat{n}_p + \cdots, \tag{9}$$

where the fermionic number operators $\hat{n}_k$ describe quasi-local integrals of motion (l-bits) coupled by diagonal matrix elements $U_{k_1 k_2 \ldots k_n}$ that decay exponentially with the localization length ξ [64]. We can directly read off the full many-particle eigenstates, which are the Fock states with respect to the l-bits $|\mathbf{n}\rangle = |\{n_k\}\rangle$, $n_k = 0, 1$, and the corresponding many-particle spectrum $E_\mathbf{n} = E(\{\mathrm{n}_k\})$.

We focus on the limit of weak interactions, where it is assumed that there exists a quasi-local transformation (adiabatic connection) between the l-bits and the local annihilation operators $\hat{a}_i$ for fermions on lattice sites i [4, 45]

$$\hat{c}_k = \sum_i u_i \hat{a}_i + \sum_{i,j,k} u_{ijk} \hat{a}_i \hat{a}_j^\dagger \hat{a}_k + \ldots, \tag{10}$$

such that the l-bit operators read $\hat{n}_k = \hat{c}_k^\dagger \hat{c}_k$. In the MBL regime with strong disorder, the coefficients u_i, u_{ijk} essentially have a local support with some exponential tails decaying on length scale ξ. It can be shown [53] that the terms that lead to particle-hole dressing u_{ijk} and all higher order terms contribute at least in first order in the interaction strength V, so for weak interactions V and strong disorder the quasi-particles are in leading order given by a single-particle transformation.

2.3. MBL system in the presence of a phonon bath

Let us now discuss the coupling of an MBL system to a phonon bath with a coupling operator $\hat{v}$ that is some single-particle operator $\hat{v} = \sum_{ij} v_{ij} \hat{a}_i^\dagger \hat{a}_j$

$$\hat{H}_{\mathrm{SB}} = \gamma \sum_{i,j} v_{ij} \hat{a}_i^\dagger \hat{a}_j \otimes \sum_\alpha \lambda_\alpha (\hat{b}_\alpha + \hat{b}_\alpha^\dagger). \tag{11}$$

The form of $\hat{H}_{\mathrm{SB}}$ induces quantum jumps between eigenstates of $\hat{H}$ and the corresponding dissipator is given by

$$\mathcal{D}_{\mathrm{heat}}(\hat{\rho}) = \sum_{\mathbf{n},\mathbf{n}'} \left(\hat{L}_{\mathbf{n}'\mathbf{n}} \hat{\rho} \hat{L}^\dagger_{\mathbf{n}'\mathbf{n}} - \frac{1}{2}\{\hat{L}^\dagger_{\mathbf{n}'\mathbf{n}} \hat{L}_{\mathbf{n}'\mathbf{n}}, \hat{\rho}\} \right), \tag{12}$$

with $\hat{L}_{\mathbf{n}'\mathbf{n}} = \sqrt{R_{\mathbf{n}'\mathbf{n}}}\, |\mathbf{n}'\rangle\langle\mathbf{n}|$ describing the jump from Fock state $|\mathbf{n}\rangle$ to the state $|\mathbf{n}'\rangle$. The associated jump rate is then given by

$$R_{\mathbf{n}'\mathbf{n}} = 2\pi\gamma^2 |\langle \mathbf{n}'|\hat{v}|\mathbf{n}\rangle|^2 g(E_{\mathbf{n}'} - E_\mathbf{n}), \tag{13}$$

with $g(E)$ the bath correlation function (equation (7)). Note that generally, in the full spectrum of a quantum many-body system one expects that a large number of close degeneracies occur, which violates the validity condition of the rotating-wave approximation [34]. However, for MBL systems in the limit of weak interactions and strong disorder that we are aiming at, we will find significant rates only for processes, where one or at most a few excitations are transferred. Moreover, typically the bath will transfer excitations only between nearby l-bits, since v_{ij} decays on the correlation lengths of the bath. Both together leads to a much milder condition.

For weak interactions and strong disorder, particle-hole dressing is suppressed, such that the transformation to the l-bits effectively becomes a single-particle transformation

$$\hat{c}_k^\dagger \approx \sum_i \psi_k(i)\hat{a}_i^\dagger. \tag{14}$$

In this case, the dissipator simplifies to

$$\mathcal{D}_{\text{heat}}(\hat{\rho}) = \sum_{\mathbf{n},k,q}\left[\hat{L}_{qk}(\mathbf{n})\hat{\rho}\hat{L}_{qk}^\dagger(\mathbf{n}) - \frac{1}{2}\{\hat{L}_{qk}^\dagger(\mathbf{n})\hat{L}_{qk}(\mathbf{n}),\,\hat{\rho}\}\right], \tag{15}$$

with $\hat{L}_{qk}(\mathbf{n}) = \sqrt{R_{\mathbf{n}_{qk},\mathbf{n}}}\,|\mathbf{n}_{qk}\rangle\langle\mathbf{n}|$ describing the jump from Fock state $|\mathbf{n}\rangle = |n_1,\ldots,n_k,\ldots,n_q,\ldots,n_M\rangle$ to the state $|\mathbf{n}_{qk}\rangle = |n_1,\ldots,n_k - 1,\ldots,n_q + 1,\ldots,n_M\rangle$ by transferring a particle from the single-particle mode k to the mode q. The fact that we neglect particle-hole dressing leads to

$$|\langle\mathbf{n}_{qk}|\hat{v}|\mathbf{n}\rangle|^2 = |\nu_{kq}|^2 n_k{}^2(1 - n_q)^2 = |\nu_{kq}|^2 n_k(1 - n_q), \tag{16}$$

with the single-particle matrix element of the coupling operator

$$|\nu_{kq}|^2 = \left|\sum_{i,j}\psi_k^*(i)v_{ij}\psi_q(j)\right|^2. \tag{17}$$

For convenience, we introduce an effective single-particle rate

$$\tilde{R}_{qk}(\mathbf{n}) = 2\pi\gamma^2|\nu_{kq}|^2 g(E_{\mathbf{n}_{qk}} - E_{\mathbf{n}}), \tag{18}$$

which in the noninteracting case, with $E_{\mathbf{n}_{qk}} - E_{\mathbf{n}} = \varepsilon_q - \varepsilon_k$, reduces to the single-particle rate $\tilde{R}_{qk}(\mathbf{n}) = R_{qk}$. This allows for the extraction of quantum statistical factors from the many-particle rate

$$R_{\mathbf{n}_{qk},\mathbf{n}} = \tilde{R}_{qk}(\mathbf{n})(1 - n_q)n_k. \tag{19}$$

This expression resembles the expression found for the ideal gas [62], where the many-particle rate is the single-particle rate R_{qk} multiplied by the occupation of the departure state n_k and the Pauli blocking factor $(1 - n_q)$ of the target state. The difference is that due to interactions, the transition rate depends on the whole configuration, rather than only on the two single-particle states involved in the transition.

2.4. MBL system in the presence of a particle reservoir

Let us now turn to the case where the system may also exchange particles with an external fermionic reservoir with temperature T and chemical potential μ. For simplicity, we again consider the regime where we can neglect particle-hole dressing. Here the system-bath Hamiltonian is given by

$$\hat{H}_{\text{SB}} = \sum_\alpha \lambda_\alpha(\hat{b}_\alpha\hat{d}^\dagger + \hat{b}_\alpha^\dagger\hat{d}), \tag{20}$$

where $\hat{d} = \sum_i \varphi(i)\hat{a}_i$ is an arbitrary single-particle mode in the system. The resulting dissipator reads

$$\mathcal{D}_{\text{part}}(\hat{\rho}) = \sum_{\alpha=\pm}\sum_{\mathbf{n},k}\left[\hat{L}_{\alpha,k}(\mathbf{n})\hat{\rho}\hat{L}_{\alpha,k}^\dagger(\mathbf{n}) - \frac{1}{2}\{\hat{L}_{\alpha,k}^\dagger(\mathbf{n})\hat{L}_{\alpha,k}(\mathbf{n}),\,\hat{\rho}\}\right], \tag{21}$$

where $\hat{L}_{+,k}(\mathbf{n}) = \sqrt{\Gamma_{+,\mathbf{n}}}\,|\mathbf{n}\rangle\langle\mathbf{n}_{k\downarrow}|$ and $\hat{L}_{-,k}(\mathbf{n}) = \sqrt{\Gamma_{-,\mathbf{n}}}\,|\mathbf{n}_{k\downarrow}\rangle\langle\mathbf{n}|$, with $|\mathbf{n}_{k\downarrow}\rangle = |n_1,\ldots n_k - 1,\ldots\rangle$ being the Fock state obtained by removing one particle from mode k. The jump rates $\Gamma_{\pm,\mathbf{n}}$ are given by

$$\Gamma_{\pm,\mathbf{n}} = \nu_k(\mathbf{n})g_{\text{F}}^{\pm}(E_{\mathbf{n}} - E_{\mathbf{n}_{k\downarrow}}), \tag{22}$$

with the coupling matrix element

$$\nu_k(\mathbf{n}) = |\langle\mathbf{n}_{k\downarrow}|\hat{d}|\mathbf{n}\rangle|^2 = \left|\sum_i \varphi^*(i)\psi_k(i)\right|^2 n_k \equiv \eta(k)n_k, \tag{23}$$

and the bath-correlation function for the particle exchange with the fermionic bath

$$g_{\text{F}}^{+}(E) = J(E)f(E,\,\mu,\,T), \tag{24}$$

$$g_{\text{F}}^{-}(E) = J(-E)[1 - f(-E,\,\mu,\,T)], \tag{25}$$

where $f(E,\,\mu,\,T) = (\mathrm{e}^{(E-\mu)/T} + 1)^{-1}$ is the Fermi distribution of the bath.

3. Interacting Anderson insulator as quantum wire

We benchmark the explained method by studying a disordered extended Hubbard chain of spinless fermions (figure 1). The system Hamiltonian [65–67] reads

$$\hat{H} = \hat{H}_0 + V \sum_{i=1}^{M-1} \hat{a}_i^\dagger \hat{a}_i \hat{a}_{i+1}^\dagger \hat{a}_{i+1}, \tag{26}$$

with the single-particle term given by

$$\hat{H}_0 = -J \sum_{i=1}^{M-1} (\hat{a}_i^\dagger \hat{a}_{i+1} + \hat{a}_{i+1}^\dagger \hat{a}_i) + \sum_{i=1}^{M} w_i \hat{a}_i^\dagger \hat{a}_i, \tag{27}$$

where $\hat{a}_i$ ($\hat{a}_i^\dagger$) is the fermionic annihilation (creation) operator at site i in a chain of length M. Moreover, w_i are random fields uniformly distributed in the interval $[-W, W]$, J and V are respectively the hopping and the interaction strength. $\hat{H}_0$ describes the noninteracting Anderson-model [68] (see appendix A.3) and all its single-particle eigenstates are exponentially localized for any amount of disorder W [69]. For $V \neq 0$ the model has an MBL transition [3–6]. At large disorder $W \gg V$, the system is in the MBL phase and it is a perfect insulator, while for weak disorder $W \ll V$ the system is ergodic, describing a thermal phase. We couple the system to two leads at the ends of the chain. The leads, which exchange particles with the system, have the same temperature T but different chemical potentials (μ_L and μ_R), inducing thus particle transport through the chain. Moreover, the system is also coupled to a global thermal bath also at temperature T (unless stated otherwise), with which it exchanges energy, as sketched in figure 1.

We are interested in the limit of weak interactions at strong disorder, where in leading order l-bits can be approximated by the noninteracting Anderson operators [53], so that we arrive at the approximate Hamiltonian

$$\hat{H}_{\text{app}} = \sum_k \varepsilon_k \hat{n}_k + \frac{1}{2} \sum_{k,q} U_{kq} \hat{n}_k \hat{n}_q. \tag{28}$$

Here $\hat{n}_k = \hat{c}_k^\dagger \hat{c}_k$ with $\hat{c}_k^\dagger = \sum_i \psi_k(i) \hat{a}_i^\dagger$, and ε_k, ψ_k are the single-particle eigenenergies and eigenmodes, respectively. The interaction coefficients U_{kq} are given by

$$U_{kq} = -2V \sum_i [\psi_k(i)\psi_q(i)\psi_k(i+1)\psi_q(i+1) - |\psi_k(i)|^2 |\psi_q(i+1)|^2]. \tag{29}$$

Since the orbitals are exponentially localized, $\psi_k(i) \propto \mathrm{e}^{-|i-i_k|/\xi_{\text{loc}}(k)}$, with localization center i_k and the single-particle localization length ξ_{loc} [70], after a relabeling of the indexes (k, q) according to their spatial positions, we have $U_{kq} \sim V e^{-|k-q|/\xi_{\text{loc}}}$ (here ξ_{loc} is the localization length in the middle of the single-particle spectrum). This approximation (equation (28)) is equivalent to discarding the off-diagonal elements of the full Hamiltonian (equation (26)) in the non-interacting basis. Its reliability for weak interactions has been shown in [53]. Its validity is strongly supported also by the spatio-energetic anti-correlations between the single-particle Anderson orbitals. If two single-particle eigenstates are close to each other in space, their energy difference is more likely to be large, suppressing scattering events between these states. Figure 2 gives evidence of the existence of this anti-correlation, showing the distribution of the spatial distance between pairs of eigenstates $\Delta R = |\sum_i i(|\psi_k(i)|^2 - |\psi_q(i)|^2)|$ as a function of their energetic distance $\Delta E = |\varepsilon_k - \varepsilon_q|$. The distribution is mainly concentrated at the left bottom corner of figures (a)–(c), which are zoomed in (d)–(f). It is important to point out that a better approximation for the l-bits can be obtained systematically by treating the omitted matrix elements perturbatively, giving rise to higher order corrections in interaction strength [28]. Such a procedure is beyond the scope of this paper but it would not render our approach inefficient.

We couple this system to a heat reservoir via the system-bath Hamiltonian

$$\hat{H}_{\text{SB}} = \gamma \sum_i \hat{n}_i \otimes \sum_\alpha C_\alpha (\hat{b}_\alpha^{(i)\dagger} + \hat{b}_\alpha^{(i)}), \tag{30}$$

which couples each site to an independent bath of bath-correlation length zero. C_α and γ are the coupling strengths. Furthermore, we assume an Ohmic bath, with spectral density $J(E)$ proportional to E, $J(E) \propto E$. The total rate that enters in equation (15) is therefore the sum of the rates for individual heat baths that couple to a single site i only.

We investigate the transport properties of the steady state, when the system is coupled to the two leads and the thermal bath. The lead coupling is described by

$$\hat{H}_{\text{SB},L} = \sqrt{\kappa} \sum_\alpha D_\alpha (\hat{b}_\alpha^{(L)} \hat{a}_1^\dagger + \hat{b}_\alpha^{(L)\dagger} \hat{a}_1), \tag{31}$$

$$\hat{H}_{\text{SB},R} = \sqrt{\kappa} \sum_\alpha D_\alpha (\hat{b}_\alpha^{(R)} \hat{a}_M^\dagger + \hat{b}_\alpha^{(R)\dagger} \hat{a}_M). \tag{32}$$

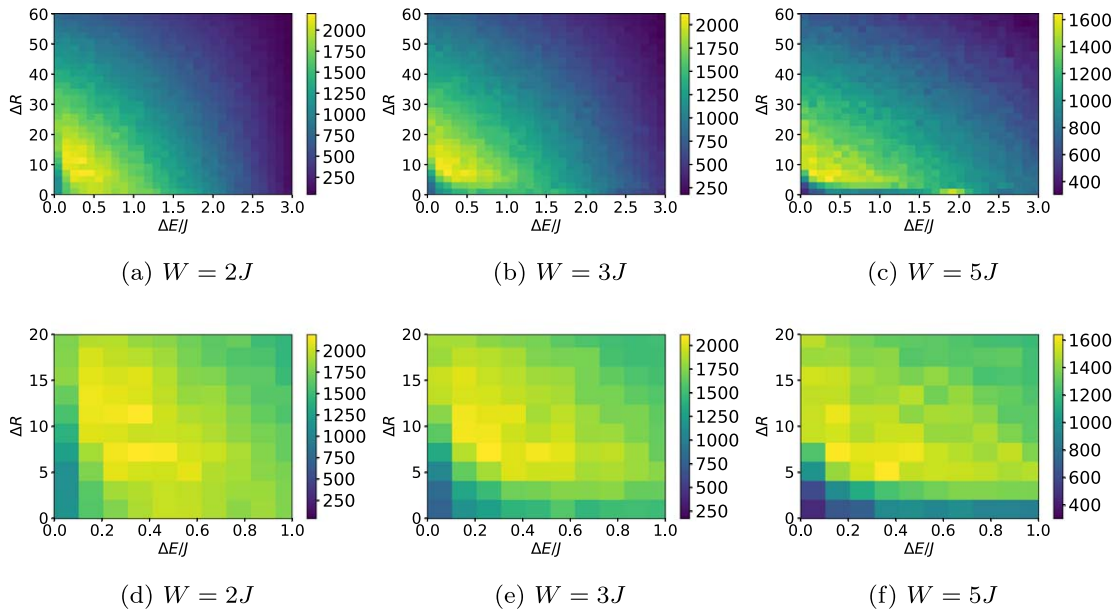

Figure 2. Distribution of the spatial distance of two eigenstates ΔR as a function of their energy difference ΔE. 1000 disorder realizations are added up. (d)–(f) are respectively the zoom-in views of (a)–(c).

The resulting coupling rates $\eta_L(k) = |\psi_k(1)|^2$, $\eta_R(k) = |\psi_k(M)|^2$ that enter in equation (23) are proportional to the value of the wavefunctions at the ends of the chain. For the leads we assume a constant density of states.

The effective single-particle energies are shifted due to interactions. Within the scope of the approximate Hamiltonian in equation (28), it is convenient to define an interaction-shifted energy operator for each l-bit

$$\hat{\tilde{\varepsilon}}_k = \varepsilon_k + \sum_q U_{kq}\hat{n}_q. \tag{33}$$

The energy difference occurring in the rate for the heat bath, equation (18), can then be expressed as

$$E_{\mathbf{n}_{qk}} - E_{\mathbf{n}} = \langle \mathbf{n}|\hat{\tilde{\varepsilon}}_q|\mathbf{n}\rangle - \langle \mathbf{n}|\hat{\tilde{\varepsilon}}_k|\mathbf{n}\rangle - U_{kq}. \tag{34}$$

For the particle reservoir, the energy difference in equation (22) is given by

$$E_{\mathbf{n}} - E_{\mathbf{n}_{k\downarrow}} = \langle \mathbf{n}|\hat{\tilde{\varepsilon}}_k|\mathbf{n}\rangle. \tag{35}$$

Note that writing energy differences in terms of $\hat{\tilde{\varepsilon}}_k$ does not constitute an additional approximation.

4. Solving the master equation

We employ two methods to compute the non-equilibrium steady state of the master equation. The first method is a quantum-jump Monte Carlo technique, which makes use of the fact that the equations of motion for the Fock-space occupation probabilities $p_{\mathbf{n}}$ can be mapped to a classical random walk. This method gives accurate results after sufficient statistical sampling. The second method consists in deriving kinetic equations of motion by employing a mean-field decomposition of density-density correlations. Importantly, both approaches are found to agree very well.

4.1. Method I: quantum-jump Monte Carlo simulation

As we discuss in section 2.1, the dynamics of the many-body occupation probabilities $p_{\mathbf{n}} = \langle \mathbf{n}|\hat{\rho}|\mathbf{n}\rangle$ decouples from the off-diagonal elements, which decay over time. For our model, the equation of motion for the probabilities is given by

$$\begin{aligned}\partial_t p_{\mathbf{n}} = &\sum_{k,q}(1-n_q)n_k[\tilde{R}_{kq}(\mathbf{n}_{qk})p_{\mathbf{n}_{qk}} - \tilde{R}_{qk}(\mathbf{n})p_{\mathbf{n}}] \\ &+ \sum_{\alpha=L,R}\sum_k \kappa\eta_\alpha(k)\{f_\alpha(\tilde{\varepsilon}_k)[n_k p_{\mathbf{n}_{k\downarrow}} - (1-n_k)p_{\mathbf{n}}] \\ &+ (1-f_\alpha(\tilde{\varepsilon}_k))[(1-n_k)p_{\mathbf{n}_{k\uparrow}} - n_k p_{\mathbf{n}}]\},\end{aligned} \tag{36}$$

where $\tilde{\varepsilon}_k = \langle \mathbf{n}|\hat{\tilde{\varepsilon}}_k|\mathbf{n}\rangle$, and we use the short notation $f_\alpha(E) = f(E, \mu_\alpha, T_\alpha)$ with $\alpha = L, R$. The first line in equation (36) describes the heat exchange processes, with the first term denoting the increase of the probability

$p_{\mathbf{n}}$ by jumping from $|\mathbf{n}_{qk}\rangle$ to the state $|\mathbf{n}\rangle$, and the second term denoting the inverse process. The second line and third line in equation (36) describe particle exchange with the leads, with the first term denoting particle gain, and the second term the particle loss.

We generalize the quantum-jump Monte-Carlo method described in [54] to the case of number-dependent single-particle rates $\tilde{R}_{qk}(\mathbf{n})$. The dynamics of the occupation probability $p_{\mathbf{n}}$ is simulated by taking random walks in the classical space composed by the Fock states $|\mathbf{n}\rangle = |n_1,\ldots,n_k,\ldots,n_M\rangle$ (not their superpositions) [62] corresponding to the given jump rates. In our case, we have two types of jumps, the first one due to the global thermal bath and the second one due to the leads. For the heat exchange processes, a jump transfers one particle from one single-particle eigenstate to another, which conserves the total particle number. For the particle exchange processes, a jump adds (or removes) a particle to (or from) one eigenstate. We perform these simulations by using a Gillespie-type algorithm (see appendix A.1). We can then compute steady state expectation values (e.g. $\langle\hat{n}_k\rangle$, $\langle\hat{n}_k\hat{n}_q\rangle$), by averaging over the long-time dynamics of many trajectories.

4.2. Method II: kinetic theory

In order to treat larger systems and to gain some intuitive understanding of the NESS, we will now derive kinetic equations of motion for the mean occupation numbers $\langle\hat{n}_l\rangle$. The time evolution of $\langle\hat{n}_l\rangle$, again for the special case of our model system, is given by

$$\frac{\mathrm{d}}{\mathrm{d}t}\langle\hat{n}_l\rangle = \mathrm{tr}[\hat{n}_l\partial_t\hat{\rho}] = \left(\frac{\mathrm{d}}{\mathrm{d}t}\langle\hat{n}_l\rangle\right)_{\mathrm{heat}} + \left(\frac{\mathrm{d}}{\mathrm{d}t}\langle\hat{n}_l\rangle\right)_{\mathrm{part}}, \tag{37}$$

with (see appendix A.2)

$$\left(\frac{\mathrm{d}}{\mathrm{d}t}\langle\hat{n}_l\rangle\right)_{\mathrm{heat}} = \sum_k[\langle\hat{\tilde{R}}_{lk}\hat{n}_k(1-\hat{n}_l)\rangle - \langle\hat{\tilde{R}}_{kl}\hat{n}_l(1-\hat{n}_k)\rangle], \tag{38}$$

and

$$\begin{aligned}\left(\frac{\mathrm{d}}{\mathrm{d}t}\langle\hat{n}_l\rangle\right)_{\mathrm{part}} &= \sum_{\alpha=L,R}\eta_\alpha(l)[\langle f_\alpha(\hat{\tilde{\varepsilon}}_l)(1-\hat{n}_l)\rangle - \langle(1-f_\alpha(\hat{\tilde{\varepsilon}}_l))\hat{n}_l\rangle] \\ &= \sum_{\alpha=L,R}\eta_\alpha(l)\langle f_\alpha(\hat{\tilde{\varepsilon}}_l) - \hat{n}_l\rangle.\end{aligned} \tag{39}$$

In equation (38), we have defined an effective rate operator

$$\hat{\tilde{R}}_{lk} = \sum_{\mathbf{n}}\tilde{R}_{lk}(\mathbf{n})|\mathbf{n}\rangle\langle\mathbf{n}|. \tag{40}$$

Using equation (34), we find

$$\hat{\tilde{R}}_{lk} = 2\pi\gamma^2|\nu_{kl}|^2 g(\hat{\tilde{\varepsilon}}_l - \hat{\tilde{\varepsilon}}_k - U_{lk}). \tag{41}$$

The effect of interactions is to modify the energy difference between the states $(\hat{\tilde{\varepsilon}}_l - \hat{\tilde{\varepsilon}}_k - U_{lk})$, implying that the transition rate depends on the whole configuration, rather than only on the two single-particle states involved in the transition $(\varepsilon_l - \varepsilon_k)$.

In order to obtain a closed set of equations in terms of mean occupation values, we employ the mean-field approximation

$$\langle\prod_{k=1}^{s}\hat{n}_{i_k}\rangle \approx \prod_{k=1}^{s}\langle\hat{n}_{i_k}\rangle, \quad \forall s, \ \text{for } i_k \neq i_q, \forall k \neq q, \tag{42}$$

giving $\langle f_\alpha(\hat{\tilde{\varepsilon}}_l)\rangle \approx f_\alpha(\langle\hat{\tilde{\varepsilon}}_l\rangle)$, $\langle g(\hat{\tilde{\varepsilon}}_l - \hat{\tilde{\varepsilon}}_k - \gamma_{lk})\hat{n}_k(1-\hat{n}_l)\rangle \simeq g(\langle\hat{\tilde{\varepsilon}}_l - \hat{\tilde{\varepsilon}}_k - \gamma_{lk}\rangle)\langle\hat{n}_k\rangle\langle 1-\hat{n}_l\rangle$. In this way, we get a set of nonlinear kinetic equations of motion

$$\frac{\mathrm{d}}{\mathrm{d}t}\langle\hat{n}_l\rangle = \sum_k[\langle\hat{\tilde{R}}_{lk}\rangle\langle\hat{n}_k\rangle(1-\langle\hat{n}_l\rangle) - \langle\hat{\tilde{R}}_{kl}\rangle\langle\hat{n}_l\rangle(1-\langle\hat{n}_k\rangle)] + \sum_{\alpha=L,R}\eta_\alpha(l)[f_\alpha(\langle\hat{\tilde{\varepsilon}}_l\rangle) - \langle\hat{n}_l\rangle]. \tag{43}$$

We obtain the equations for the NESS, by setting equation (43) to zero

$$\frac{\mathrm{d}}{\mathrm{d}t}\langle\hat{n}_l\rangle_{\mathrm{NESS}} = 0. \tag{44}$$

In the following, we will always consider the steady state and, therefore, drop the subscript NESS. Using the single-particle wavefunctions ψ_l we can find the mean occupation number (density profile) in real space

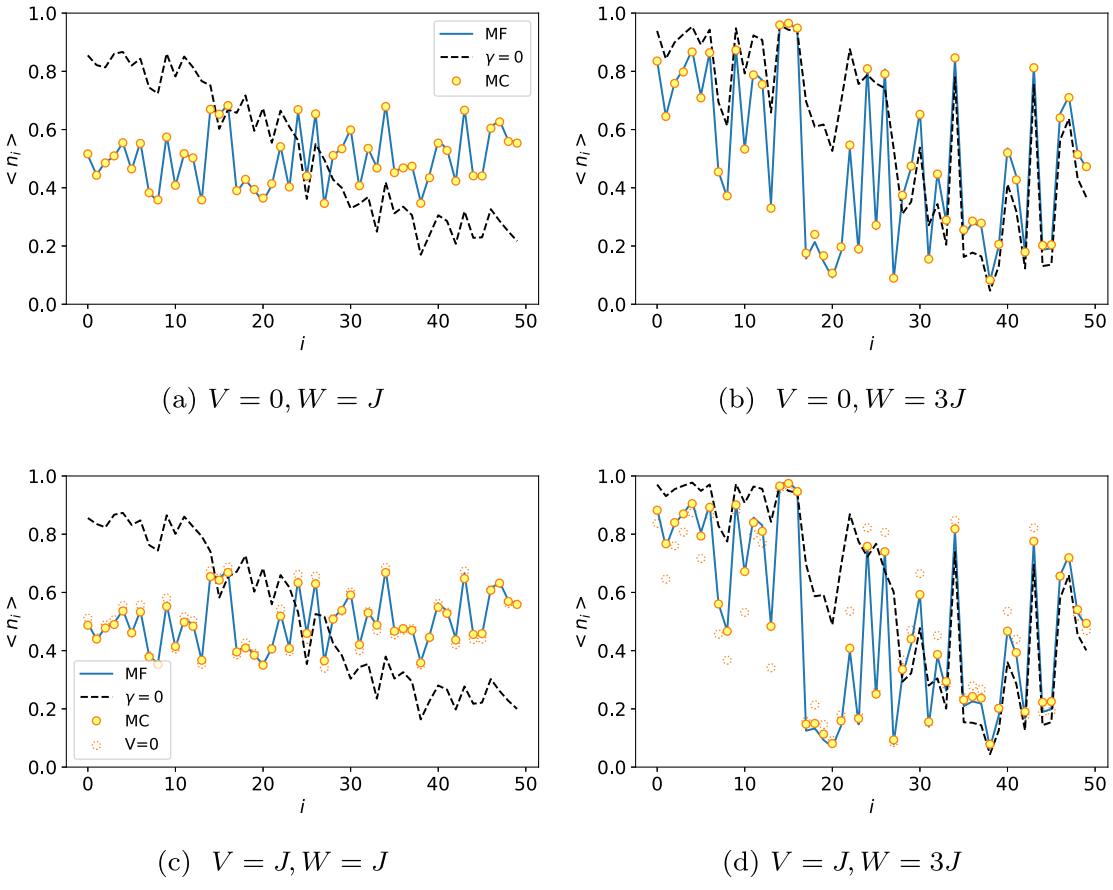

Figure 3. Density profile $\langle \hat{n}_i \rangle$ as a function of site i. The solid lines are the results from the kinetic theory and the dashed lines are the results in the absence of the global thermal bath (obtained by substituting equation (46) into (45)). The markers denote the averaged results over 1000 trajectories of quantum-jump Monte-Carlo (MC) simulations. The open circles in (c), (d) are the results with $V = 0$, as shown in (a), (b). The parameters are $M = 50, \gamma^2 = 0.01J, \kappa = 0.1\gamma^2, T = J$ and $\mu_L = \bar{\mu} + \delta\mu/2$, $\mu_R = \bar{\mu} - \delta\mu/2$, with $\delta\mu = 5J$, and $\bar{\mu}$ is set to make $N = M/2 = 25$.

$$\langle \hat{n}_i \rangle = \sum_{l=1}^{M} |\psi_l(i)|^2 \langle \hat{n}_l \rangle. \tag{45}$$

The nonlinear term in equation (43) prevents us from finding an analytic solution. However, in the absence of the global thermal bath ($\gamma = 0$), the solution of equation (44) is given by

$$\langle \hat{n}_l \rangle_{\gamma=0} = \frac{\eta_L(l) f_L(\langle \hat{\tilde{\varepsilon}}_l \rangle) + \eta_R(l) f_R(\langle \hat{\tilde{\varepsilon}}_l \rangle)}{\eta_L(l) + \eta_R(l)}. \tag{46}$$

Let us compare the methods described in sections 4.1 and 4.2 by computing the density profile $\langle \hat{n}_i \rangle$, which also determines the current to be discussed later. Figure 3 shows the density profile $\langle \hat{n}_i \rangle$ obtained by numerically solving the kinetic equations (equation (44), solid lines) and the one calculated using the quantum-jump Monte-Carlo technique (equation (36), markers). The two results are almost indistinguishable both for the noninteracting and the interacting case. The chemical potentials in the leads are taken equal to $\mu_{L,R} = \bar{\mu} \pm \delta\mu/2$ with relatively large chemical potential difference $\delta\mu = 5J$, and $\bar{\mu}$ is fixed so that the system is at half-filling ($\langle \hat{N} \rangle = M/2$, where $\hat{N}$ counts the total number of particles). Later on, we will use only small chemical potential offsets $\delta\mu$, in order to compute conductivities. The large difference between the chemical potentials produces a density gradient in the absence of the global thermal bath ($\gamma = 0$), as shown in figure 3 (black dashed lines). The presence of the global thermal bath, which induces phonon-assisted tunneling, erases this gradient for weak disorder, as shown in (a) and (c). Furthermore, by increasing the disorder strength W, which prompts the localization of the wavefunctions and thus the suppression of particle tunneling, the density gradient is restored, as shown in figures 3(b) and (d).

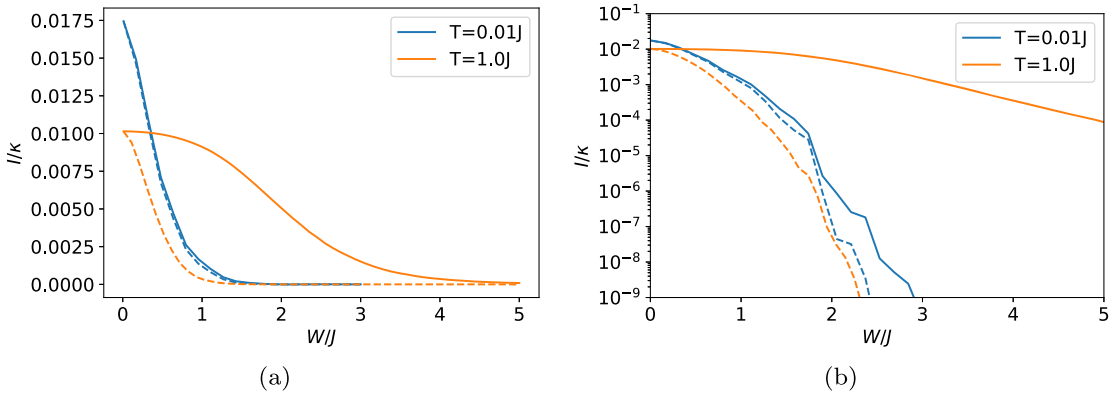

Figure 4. Current I as a function of the disorder strength W. The results are averaged over 1000 disorder realizations. The solid lines are obtained from the kinetic equations and the dashed lines are the results without coupling the system to the global bath (equation (48)). The parameters are system size $M = 100$, dissipation rate $\kappa = 0.1\gamma^2$, interaction strength $V = 0$, and $\mu_L = \bar{\mu} + \delta\mu/2$, $\mu_R = \bar{\mu} - \delta\mu/2$, with chemical potential imbalance $\delta\mu = 0.1J$, and $\bar{\mu}$ is set to make $N = M/2 = 50$. Except when otherwise stated, we will take the same parameters for the rest of the work.

5. Results I: observation of VRH for noninteracting Fermions in a microscopic model

We investigate the particle current in the NESS, which is defined as the net particle flow at the ends of the chain

$$I = \sum_{l=1}^{M} \eta_L(l)[f_L(\langle\hat{\tilde{\varepsilon}}_l\rangle) - \langle\hat{n}_l\rangle] = -\sum_{l=1}^{M} \eta_R(l)[f_R(\langle\hat{\tilde{\varepsilon}}_l\rangle) - \langle\hat{n}_l\rangle]. \tag{47}$$

Having shown that the kinetic equations, equation (43), are reliable, we now use this approach to study the dependence of the current I, equation (47), on disorder strength W, on temperature T of the bath, and on interaction strength V. As shown in appendix A.4, for the current, the results of the kinetic equations also agree very well with those from Monte-Carlo simulations. In the following, we will only show disorder-averaged results of the kinetic theory.

5.1. Transport as a function of disorder strength W

In the absence of the thermal bath ($\gamma = 0$), the current in the NESS is given by

$$I_{\gamma=0} = \sum_{l=1}^{M} [f_L(\langle\hat{\tilde{\varepsilon}}_l\rangle) - f_R(\langle\hat{\tilde{\varepsilon}}_l\rangle)] \frac{\eta_L(l)\eta_R(l)}{\eta_L(l) + \eta_R(l)}, \tag{48}$$

which is obtained by substituting the solution of the occupation numbers, equation (46), into (47). The terms of $I_{\gamma=0}$ are proportional to the product $\eta_L(l)\eta_R(l) \propto |\psi_l(1)|^2|\psi_l(M)|^2 \sim \exp(-4M/\xi_{\text{loc}})$, where for strong disorder $\xi_{\text{loc}} \sim 1/\log(W)$. This implies that without coupling to a thermal environment the current will dramatically decay with disorder strength. This is confirmed in figure 4 (dashed lines), where the behavior of the current is shown as a function of W for the non-interacting chain of $M = 100$ lattice sites. Here and in the following, we consider a weak chemical potential difference $\delta\mu = 0.1J$. Figure 4 also reports the case in which the thermal bath is present ($\gamma \neq 0$), showing that the presence of a global thermal bath enhances transport for sufficiently large T.

5.2. Transport as a function of temperature T

In this section we study the dependence of the current I on temperature T and disorder strength W for the noninteracting case. Figure 5(a) shows the current I as a function of T for a fixed system size ($M = 100$) for several values of W, while figure 5(b) shows I for a fixed disorder strength W for several system sizes M. We can distinguish three distinct regimes according to the value of the temperature. At 'low' temperatures T, the current approaches the result obtained in the absence of the global bath ($\gamma = 0$, dotted lines). In the intermediate temperature regime, the behavior of the current is well predicted by Mott's law for VRH [55], $I \propto \exp(-\sqrt{T_0/T})$. Finally, at 'high' temperatures ($T \gg J$), I decreases as a function of T.

Note that the locations of the three regions depend on various parameters, such as the disorder strength W (as shown in figure 5(a)), the coupling to the leads κ, and so on. The independence of the current on temperature in the 'low' temperature regime is due to the suppression of heat exchange, which can be inferred from the good agreement of the results with that without coupling to the global thermal bath (equation (48), dotted lines). Nevertheless, the remaining current ($T \to 0$) is a finite system size effect [71]. Indeed, as $T \to 0$, $I_{\gamma=0}$ decays

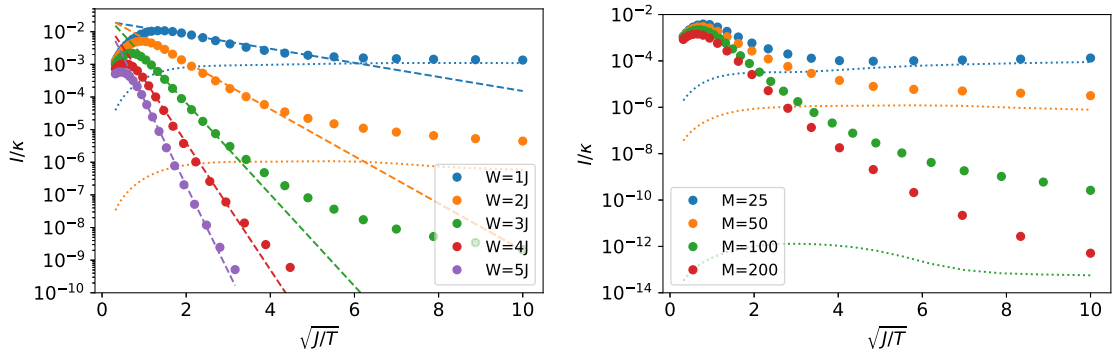

(a) $M = 100$ (b) $W = 3J$

Figure 5. Current I as a function of the temperature T of the bath for various disorder strengths with $M = 100$ (a) and for various system sizes with $W = 3J$ (b). The dashed lines are fitting curves according to $I = I_s e^{-\sqrt{T_0/T}}$ using the data with T ranging from $0.1J$ to J. The dotted lines are the results in the absence of the global heat-exchange bath (equation (48)).

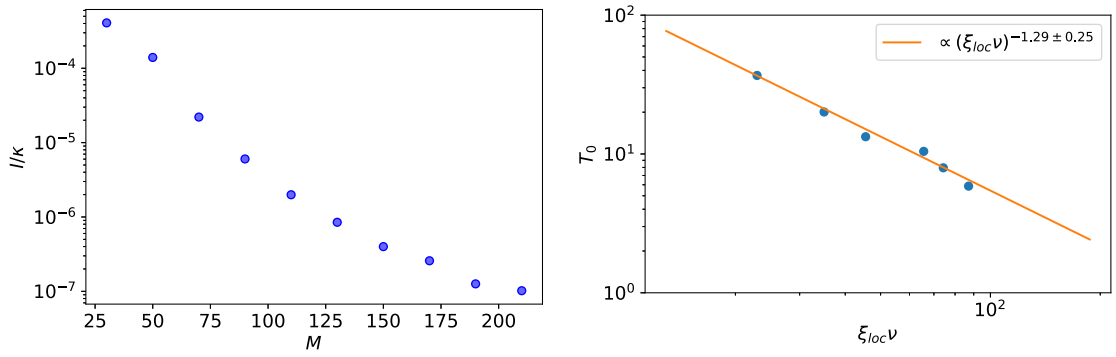

(a) $T = 0.02J, W = 2J$ (b)

Figure 6. (a) Current I at low temperature $T = 0.02J$ as a function of system size M. (b) Mott temperature T_0 (obtained from fitting) as a function of the localization length $\xi_{\rm loc}$ times the density of states ν at $k = M/2$.

exponentially with system size M, as shown in figure 6(a). For a given system size, $I_{\gamma=0}$ depends on the disorder strength, and as expected it is smaller for stronger disorder (figure 5(a)).

The intermediate-temperature VRH regime can be understood using the following argument due to Mott [55]. Let us consider the hop between states with localization centers separated by the distance ΔR and with energy difference ΔE. On the one hand, the probability to hop is proportional to the envelop overlap between the two states, thus it decays exponentially with the distance ΔR [$\sim \exp(-2\Delta R/\xi_{\rm loc})$]. On the other hand, the probability to produce excitations of order ΔE due to the presence of the heat bath is given by the Boltzmann factor $\exp(-\Delta E/T)$. This leads us to assume that the current (conductivity) to leading order is given by

$$I \sim e^{-2\Delta R/\xi_{\rm loc} - \Delta E/T}. \tag{49}$$

As already mentioned, the spatial distance ΔR and the energy separation ΔE, are not independent, but show clear anticorrelations (figure 2), which shall be captured by $\Delta R \sim (\Delta E \nu)^{-1}$, where ν is the density of states. Thus, the current is determined by the competition between the overlap term $\exp(-2\Delta R/\xi_{\rm loc})$ which favors short hops and the energy activation $\exp(-\Delta E/T)$, which favors long hops. Maximizing this probability over ΔE, one finds in one spatial dimension

$$I \propto e^{-2\Delta R_0/\xi_{\rm loc}} = e^{-\sqrt{T_0/T}} = e^{-\Delta E_0/T}, \tag{50}$$

with Mott's hopping length $\Delta R_0 = \sqrt{\xi_{\rm loc}/(2T\nu)}$ and Mott's temperature $T_0 = 2/(\xi_{\rm loc}\nu)$. Moreover, Mott's hopping energy $\Delta E_0 = \sqrt{T_0 T}$ is the energy scale that defines the width of the energy interval of the activated eigenenergies. Note that the VRH mechanism relies on the continuous density of states for the phonon bath, which ensures the ability of the particles to draw energy from phonons for hopping [72]. By fitting the current in the intermediate temperature regime to Mott's law $I = I_s \exp(-\sqrt{T_0/T})$, we can extract T_0. Figure 6(b) shows T_0 as a function of $\xi_{\rm loc}\nu$, where $\xi_{\rm loc}$ is the single-particle localization length in the middle of the energy-band

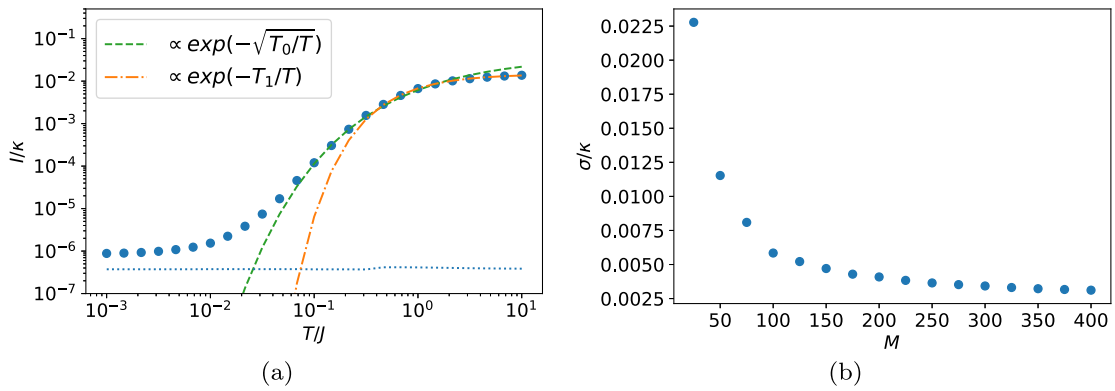

Figure 7. (a) Current I as a function of the temperature T for the global bath. Here, the temperatures for the local baths are fixed at $0.01J$. The dotted line is the result in the absence of the global thermal bath, i.e. equation (48). The disorder strength is $W = 2J$. (b) Conductivity σ as a function of system size M. Other parameters are $T = 0.5J$, disorder strength $W = 5J$.

($\varepsilon_k \sim 0$). We find that at strong disorder, $T_0 \propto (\xi_{\rm loc}\nu)^{-1.29\pm0.25}$, agreeing rather well with the Mott's prediction $\propto(\xi_{\rm loc}\nu)^{-1}$.

Finally, in the 'high' temperature regime, we attribute the decrease of the current with respect to temperature to the fact that the difference between the Fermi distributions of the leads ($f_L(\langle\hat{\tilde{\varepsilon}}_l\rangle) - f_R(\langle\hat{\tilde{\varepsilon}}_l\rangle)$) is washed out. To support this idea, we fix the temperature of the leads at $T_L = T_R = 0.01J$. In this case, the current I increases with the temperature of the global thermal bath T as $\exp(-T_1/T)$ in the 'high' temperature regime, as shown in figure 7(a). The reason is that the thermal energy T is so high that, despite of their large energy separation, already activated hopping between nearest neighboring localized orbitals dominates over the VRH behavior.

From the current, we can deduce the conductance $G = I/\delta\mu$, as well as the conductivity

$$\sigma = GM = \frac{IM}{\delta\mu}. \tag{51}$$

Figure 7(b) shows the conductivity σ at temperature $T = 0.5J$ as a function of the system size M for $W = 5J$. We can observe that σ converges to a finite value in the limit $M \to \infty$.

6. Results II: VRH for weakly interacting Fermions

Let us now discuss transport in the presence of weak interactions, for which the system is in the MBL phase. Here, we exploit the advantages of our method, allowing for the treatment of interacting systems in the presence of a thermal environment. All of our results are obtained in the limit of weak interactions and strong disorder in which the approximation (equation (28)) is justified.

6.1. Transport as a function of temperature T

Figure 8(a) shows the temperature dependence of the current for several interaction strengths V. Interestingly, also for the interacting case ($V \neq 0$), we find a regime of temperatures, where the current is explained by Mott's law ($I \sim \exp(-\sqrt{T_0/T})$), in agreement with the analytical prediction of [56]. We find that in this VRH regime, attractive interactions (blue dashed line) enhance transport, while for repulsive interactions (orange dashed–dotted line) the current decreases. This means that the interaction changes Mott's temperature T_0. Figure 8(b) shows the dependence of Mott's temperature T_0 on the interaction strength V. We can see how attractive interactions decrease T_0, while repulsive interactions increase T_0.

Can we understand this behavior? From our previous discussion we know that T_0 depends on the localization length $\xi_{\rm loc}$ and on the density of states ν. However, within our approximation, the localization length is not affected by the interactions. We should, therefore, be able to explain the interaction-induced shift of Mott's temperature in terms of interaction-induced shifts of the density of states.

6.2. Interaction-shifted density of states

In figure 9(a), we show the energies $\langle\hat{\tilde{\varepsilon}}_k\rangle$ in the steady state for $V = -0.4J$, $V = 0$ and $V = 0.4J$ all at $T = 0.5J$. As expected from equation (33), repulsive interactions ($V > 0$, orange dashed–dotted line) shift the single-particle energies ε_k up (black solid line) and attractive interactions ($V < 0$, blue dashed line) decrease them. However, this does not imply a change in the average level splitting $\langle\hat{\tilde{\varepsilon}}_k - \hat{\tilde{\varepsilon}}_{k-1}\rangle$. What is crucial is rather that the interaction-dependent energy shift depends on k. The absolute value of the energy shift $\delta E_k \equiv \langle\hat{\tilde{\varepsilon}}_k\rangle - \varepsilon_k$ is

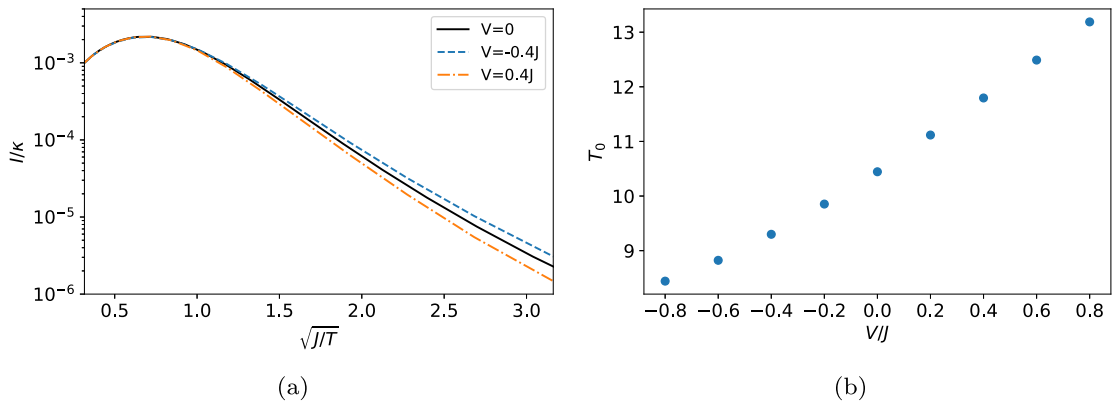

Figure 8. (a) Temperature dependence of the current for various interaction strengths V. (b) Fitted values of Mott's temperature T_0 as a function of the interaction strength V. The disorder strength is $W = 3J$.

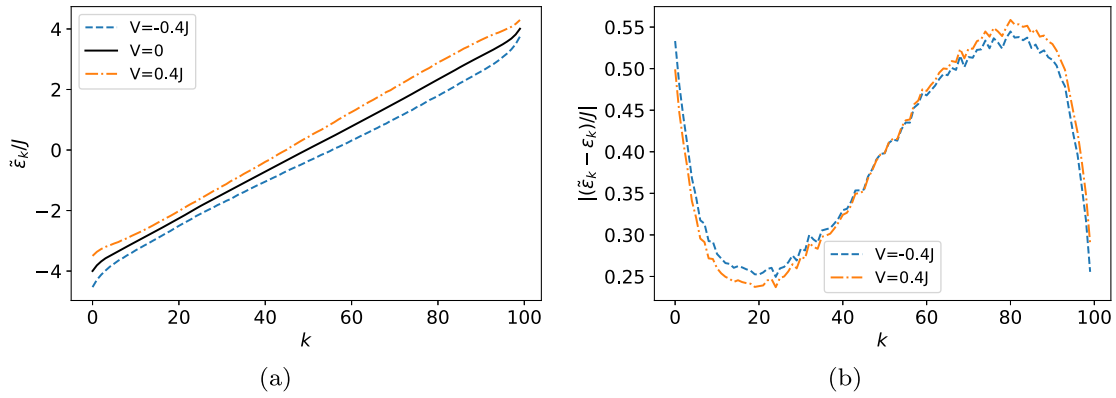

Figure 9. (a) Interaction-shifted single-particle energies $\langle\hat{\tilde{\varepsilon}}_k\rangle$ at temperature $T = 0.5J$. (b) Magnitude of the energy shift $\delta E_k \equiv \langle\hat{\tilde{\varepsilon}}_k\rangle - \varepsilon_k$.

shown in figure 9(b). For the eigenstates in the middle of the spectrum, which are the ones that contribute predominantly to the transport, the energy shift increases with energy.

This behavior can be understood from considering equation (33): The energy shift $\delta E_k = \sum_q U_{kq} \langle\hat{n}_q\rangle$ depends via $U_{kq} \sim Ve^{-|k-q|/\xi_{\rm loc}}$ on the overlap of the involved single-particle wave functions. Therefore, the main contribution to the shift originates from eigenstates that are close by in space. Now, due to the anti-correlation property between single-particle energy and spatial distance, these eigenstates q will have a large energy difference with respect to k. Thus a state k slightly above the Fermi energy will have more likely neighboring states below the Fermi energy with a large occupation probability, while a state slightly below the Fermi energy will more likely have neighboring states above the Fermi energy, with a small occupation probability. In this way, the positive/negative energy shift of repulsive/attractive interactions, will be larger for states above the Fermi level than for states below it. This implies that the level spacing between neighboring energy levels ($\langle\hat{\tilde{\varepsilon}}_k - \hat{\tilde{\varepsilon}}_{k-1}\rangle$) is increased for repulsive interactions and is decreased for attractive interactions. In other words, repulsive interactions reduce the density of states $\nu_k = 1/(\langle\hat{\tilde{\varepsilon}}_k - \hat{\tilde{\varepsilon}}_{k-1}\rangle)$ and attractive interactions enhance it.

6.3. Explanation of the change of Mott's temperature

The suspected behavior is confirmed in figure 10(a), where we show the averaged density of states (over states with k between 40 and 60), $\bar{\nu}$, as a function of interaction strength at temperature $T = 0.5J$. We can now check whether the dependence of Mott's temperature T_0 on interactions can be explained with their effect on the density of states. When we plot T_0 versus $\bar{\nu}$, as shown in figure 10(b), we observe a behavior $T_0 \propto \bar{\nu}^{-1.18\pm0.15}$, which agrees well with the predicted ν^{-1} dependency in Mott's temperature.

We would like to emphasize that the origin of Mott's law that we find for our system is different from the case of Coulomb interactions, which has been shown to lead to a VRH conductivity $\sigma \propto \exp[-(T_0/T)^{1/2}]$ independent of dimensionality due to a nonanalytic modification of the density of states near the Fermi energy [73]. In our case

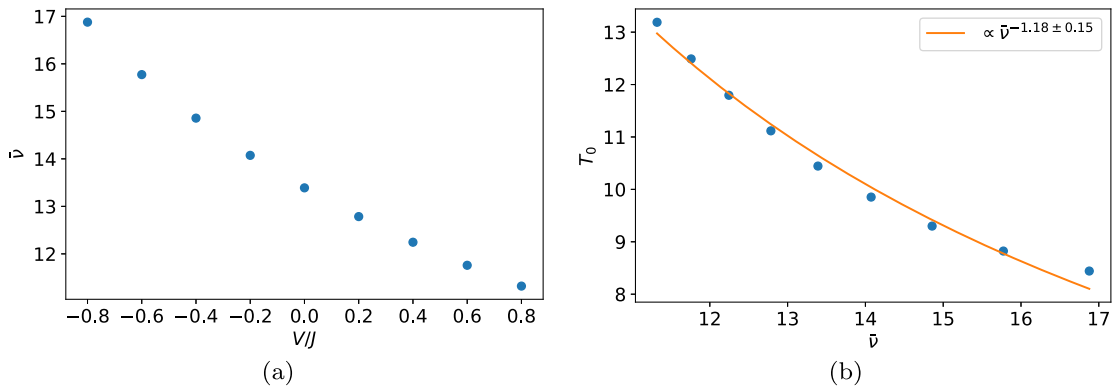

Figure 10. (a) Averaged density of states (over states with k between 40 and 60) $\bar{\nu}$ as a function of the interaction strength at temperature $T = 0.5J$. (b) Fitted values of Mott's temperature T_0 as a function of the averaged density of states $\bar{\nu}$.

of local interactions of nearest-neighbor type the density of states becomes modified only smoothly which continuously connects the interacting with the noninteracting result.

7. Conclusion

In this work we have introduced a method which allows for an efficient description of MBL systems at strong disorder and weak interactions, when weakly coupled to thermal environments. The key idea is to exploit the l-bit representation of the MBL system to derive a Born–Markov quantum master equation also for large systems. What this representation provides is the full diagonalization of the interacting many-body system essential for the description of a system in thermal environments. By making use of a recently proposed efficient approximate method controlled in the limit of strong disorder and weak interactions [53], we obtained the l-bits in leading order by a single-particle transformation. The steady state, which is diagonal in the noninteracting eigenbasis in our approximation, was then computed efficiently through classical Monte-Carlo simulation and kinetic theory.

We benchmarked our method for noninteracting systems, where we showed that our method recovers Mott's law for VRH starting from a microscopic model. Upon adding weak interactions we found that Mott's law persists while leading to perturbative corrections. We explained our observations by an interaction-induced modification of the density of states due to spatio-energetic correlations.

Concluding, our work provides a framework to study open system dynamics at mesoscopic scales for various scenarios involving MBL systems at strong disorder and weak interactions (where its l-bits can be constructed perturbatively). This includes a wide range of phenomena such as MBL-spin glasses, algebraic MBL, MBL topological phases, or time crystals.

Acknowledgments

We acknowledge support from the Deutsche Forschungsgemeinschaft (DFG) via the Research Unit FOR 2414 under project No. 277974659 and via the Gottfried Wilhelm Leibniz Prize program.

Appendix

A.1. Quantum-jump Monte Carlo simulation

We use the Gillespie algorithm [62] to perform the time evolution. For each trajectory, the system is initially prepared in a random state. Then the algorithm alternates between the following two steps. (i) Stay in a Fock state for some time. (ii) Jump to another occupation basis state. The time interval τ for staying in the current state is determined by $\tau = \min(\tau_h, \tau_g, \tau_l)$, the minimum of three values randomly drawn from exponential distribution $P(\tau_\lambda) \propto \exp[-\tau_\lambda/\bar{t}_\lambda]$ with mean dwell time for heat exchange ($\bar{t}_h$), gaining ($\bar{t}_g$) and losing ($\bar{t}_l$) a particle given by

$$\bar{t}_h^{-1} = \sum_{k,q} R_{\mathbf{n}_{qk},\mathbf{n}},$$
$$\bar{t}_g^{-1} = \sum_{k} \sum_{\alpha=L,R} \eta_\alpha(k) f_\alpha(\tilde{\varepsilon}_k),$$
$$\bar{t}_l^{-1} = \sum_{k} \sum_{\alpha=L,R} \eta_\alpha(k)(1 - f_\alpha(\tilde{\varepsilon}_k)). \tag{52}$$

According to the choice made, the corresponding jump operation is performed. Specifically, if $\tau = \tau_h$, which means heat exchange process is chosen, then a particle is transferred from a randomly drawn departure mode k to the randomly drawn target mode q. This single-particle jump has the probability $P(k \to q, \mathbf{n}) = \bar{t}_h R_{\mathbf{n}_{qk},\mathbf{n}}$. If pumping is chosen, with $\tau = \tau_g$, a particle is added to a mode randomly drawn with probability $P(k) = \bar{t}_g \sum_{\alpha=L,R} \eta_\alpha(k) f_\alpha(\tilde{\varepsilon}_k)$. Likewise, the particle loss process is performed when $\tau = \tau_l$. These two steps are repeated until the desired evolution time is reached.

An ensemble of trajectories is calculated individually, from which the wavefunctions $|\mathbf{n}^{(\lambda)}(t)\rangle$ obtained are then used to compute the expectation value of an observable O as

$$\langle O(t)\rangle = \frac{1}{L} \sum_{\lambda=1}^{L} \langle \mathbf{n}^{(\lambda)}(t)|O|\mathbf{n}^{(\lambda)}(t)\rangle. \tag{53}$$

A.2. Derivation of equations (38) and (39) in the main text

The time evolution of the mean occupation due to heat exchange is governed by

$$\left(\frac{\mathrm{d}}{\mathrm{d}t}\langle \hat{n}_l\rangle\right)_{\text{heat}} = \frac{1}{2} \sum_{\mathbf{n},k,q} R_{\mathbf{n}_{qk},\mathbf{n}} \mathrm{tr}\{[2\hat{L}_{qk}^\dagger(\mathbf{n})\hat{n}_l\hat{L}_{qk}(\mathbf{n}) - \hat{n}_l\hat{L}_{qk}^\dagger(\mathbf{n})\hat{L}_{qk}(\mathbf{n}) - \hat{L}_{qk}^\dagger(\mathbf{n})\hat{L}_{qk}(\mathbf{n})\hat{n}_l]\rho\}, \tag{54}$$

with

$$\begin{aligned} &2\hat{L}_{qk}^\dagger(\mathbf{n})\hat{n}_l\hat{L}_{qk}(\mathbf{n}) - \hat{n}_l\hat{L}_{qk}^\dagger(\mathbf{n})\hat{L}_{qk}(\mathbf{n}) - \hat{L}_{qk}^\dagger(\mathbf{n})\hat{L}_{qk}(\mathbf{n})\hat{n}_l \\ &= 2|\mathbf{n}\rangle\langle\mathbf{n}_{qk}|\hat{n}_l|\mathbf{n}_{qk}\rangle\langle\mathbf{n}| - \hat{n}_l|\mathbf{n}\rangle\langle\mathbf{n}| - |\mathbf{n}\rangle\langle\mathbf{n}|\hat{n}_l. \end{aligned} \tag{55}$$

Let us assume that Fock state $|\mathbf{n}\rangle$ has n_l particle in l mode, i.e.

$$\hat{n}_l|\mathbf{n}\rangle = n_l|\mathbf{n}\rangle. \tag{56}$$

Then it is easy to verify that for state $|\mathbf{n}_{qk}\rangle$, which is obtained from state $|\mathbf{n}\rangle$ by transferring a particle from k mode to q mode, there is the following property

$$\hat{n}_l|\mathbf{n}_{qk}\rangle = (n_l + \delta_{q,l} - \delta_{k,l})|\mathbf{n}_{qk}\rangle. \tag{57}$$

By using equations (56) and (57), we can reduce equation (55) to

$$2\hat{L}_{qk}^\dagger(\mathbf{n})\hat{n}_l\hat{L}_{qk}(\mathbf{n}) - \hat{n}_l\hat{L}_{qk}^\dagger(\mathbf{n})\hat{L}_{qk}(\mathbf{n}) - \hat{L}_{qk}^\dagger(\mathbf{n})\hat{L}_{qk}(\mathbf{n})\hat{n}_l = 2(\delta_{q,l} - \delta_{k,l})|\,\mathbf{n}\rangle\langle\mathbf{n}|. \tag{58}$$

Substituting it into equation (54), we obtain

$$\left(\frac{\mathrm{d}}{\mathrm{d}t}\langle \hat{n}_l\rangle\right)_{\text{heat}} = \sum_{\mathbf{n},k,q} R_{\mathbf{n}_{qk},\mathbf{n}}(\delta_{q,l} - \delta_{k,l})p_{\mathbf{n}} = \sum_{\mathbf{n},k}(p_{\mathbf{n}}R_{\mathbf{n}_{lk},\mathbf{n}} - p_{\mathbf{n}}R_{\mathbf{n}_{kl},\mathbf{n}}). \tag{59}$$

It then reduces to equation (38) by using equations (19) and (40) in the main text.

Likewise, by making use of

$$\begin{aligned} 2\hat{L}_k\hat{n}_l\hat{L}_k^\dagger - \hat{n}_l\hat{L}_k\hat{L}_k^\dagger - \hat{L}_k\hat{L}_k^\dagger\hat{n}_l &= 2\delta_{k,l}|\mathbf{n}_{k\downarrow}\rangle\langle\mathbf{n}_{k\downarrow}|, \\ 2\hat{L}_k^\dagger\hat{n}_l\hat{L}_k - \hat{n}_l\hat{L}_k^\dagger\hat{L}_k - \hat{L}_k^\dagger\hat{L}_k\hat{n}_l &= -2\delta_{k,l}|\mathbf{n}\rangle\langle\mathbf{n}|, \end{aligned} \tag{60}$$

we can obtain equation (39) in the main text.

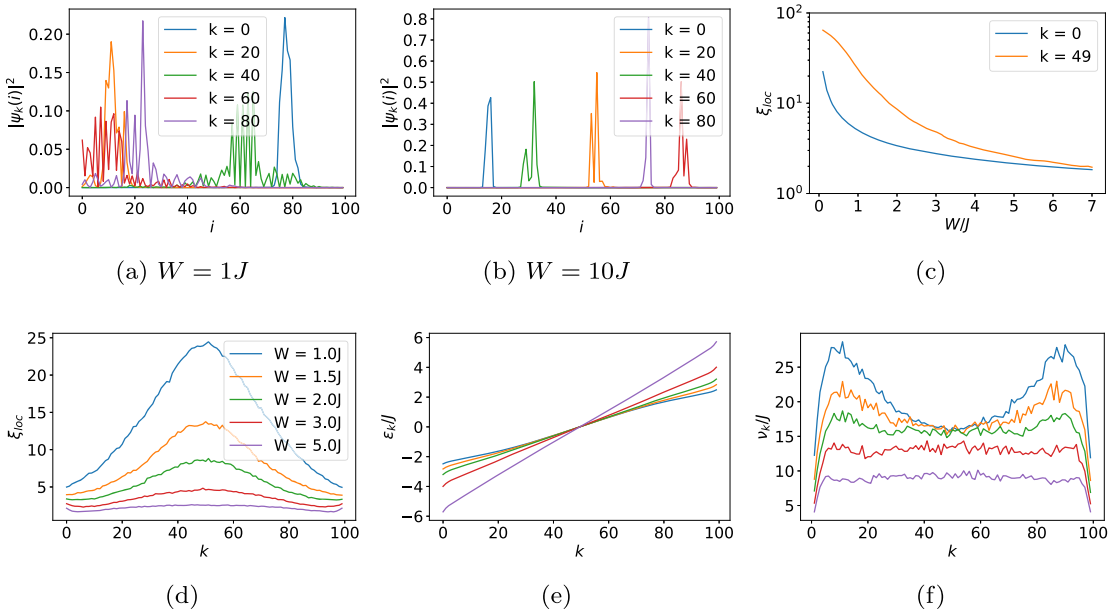

Figure A1. (a), (b) Show some selected eigenstates for the Hamiltonian (27) at different disorder strengths. (c) and (d) show the dependence of localization length $\xi_{\rm loc} \equiv 1/\sum_i |\psi_k(i)|^4$ of the eigenstates $\psi_k(i)$ on the disorder strength W and the eigenstate label k. (e) Shows the eigenenergies ε_k for some values of W. (f) Shows the density of state $\nu_k \equiv 1/(\varepsilon_k - \varepsilon_{k-1})$. System size is $M = 100$.

A.3. Anderson localization $V = 0$

In this section we show some further data concerning the non-interacting system. A straightforward basis transformation recasts $\hat{H}_0$ into the diagonalized form $\hat{H}_0 = \sum_k \varepsilon_k \hat{n}_k$ with $\hat{n}_k = \hat{c}_k^\dagger \hat{c}_k$ and $\hat{c}_k^\dagger = \sum_i \psi_k(i)\hat{a}_i^\dagger$, which creates a particle in the single-particle eigenstate $|k\rangle = \sum_i \psi_k(i)|i\rangle$ with energy ε_k that are distributed between $-2J - \mathrm{W}$ and $2J + W$, as shown in figure A1(e).

Figures A1(a), (b) show some selected eigenstates for two different disorder strengths. It is clear that as disorder becomes stronger, the wavefunctions become more localized. To characterize the localization of the wavefunction, we define the localization length using the inverse participation ratio $\xi_{\rm loc} \equiv 1/\sum_i |\psi_k(i)|^4$. As shown in figure A1(c), $\xi_{\rm loc}$ decays rapidly as disorder increases. Moreover, it also depends on the eigenenergy, as shown in figure A1(d), and $\xi_{\rm loc}$ has its maximum in the center of the energy-band (figure A1(e)). The density of states $\nu_k \equiv 1/(\varepsilon_k - \varepsilon_{k-1})$ (inverse of the energy gap between neighboring eigenstates) also depends on the disorder strength W. From figure A1(f), it is clear that larger values of W lead to a smaller density of states.

A.4. Comparison of the current from kinetic theory and quantum Monte-Carlo simulation

Figure A2(a) shows the current as a function of disorder strength W. The kinetic theory results (solid lines) agree well with the results obtained from quantum-jump Monte-Carlo simulation (markers). The agreement is better for lower temperature and weaker disorder. The reason is that the error of the Monte-Carlo simulation scales as $\Delta I/\sqrt{N_{\rm MC}}$, with $N_{\rm MC}$ being the number of trajectories for the Monte-Carlo simulation and ΔI the fluctuation of the current. From (b) we can see that, the fluctuation of the current ΔI increases with disorder strength W and temperature T. In addition, as shown in (a), the mean value of the current decreases with increasing W. These imply that to maintain a small relative error, much more trajectories are needed for stronger disorder and higher temperature. In other words, for a given number of trajectories, which is 1000 in our numerical calculation, the error of Monte-Carlo simulation will be larger for stronger disorder and higher temperature.

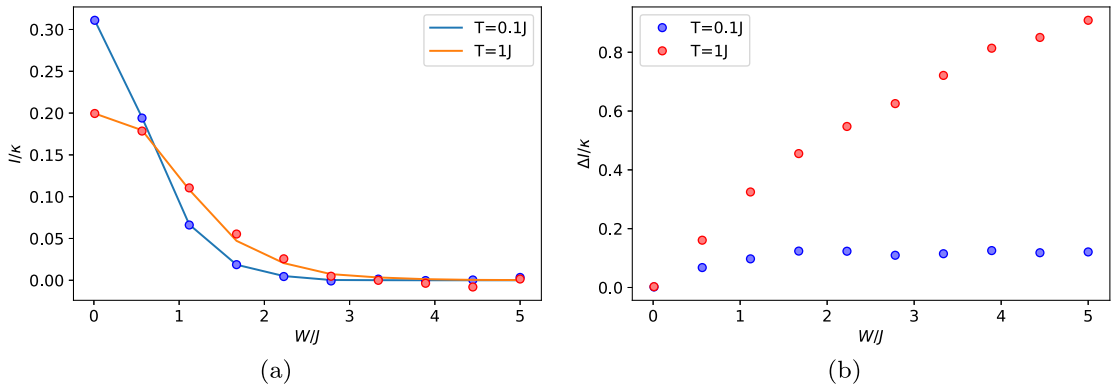

Figure A2. The current (a) and its fluctuation (b) as a function of the disorder strength W. The solid lines are the results of kinetic theory. The makers denote the results of quantum Monte-Carlo simulation. The results are averaged over 20 disorder realizations. For a given disorder configuration, the fluctuation of the current is given by $(\Delta I)_j = \sqrt{\langle I^2\rangle_j - \langle I\rangle_j^2}$, where the average $\langle\cdot\rangle$ is taken over 1000 trajectories of Monte-Carlo simulations. The parameters are: system size $M = 50$, dissipation rate $\kappa = \gamma^2$, interaction strength $V = 0$, chemical potential imbalance $\delta\mu = J$.

ORCID iDs

Ling-Na Wu https://orcid.org/0000-0003-4722-5883
Markus Heyl https://orcid.org/0000-0002-7126-1836
André Eckardt https://orcid.org/0000-0002-5542-3516

References

[1] Basko D M, Aleiner I L and Altshuler B L 2006 *Ann. Phys.* **321** 1126–205
[2] Gornyi I V, Mirlin A D and Polyakov D G 2005 *Phys. Rev. Lett.* **95** 206603
[3] Altman E and Vosk R 2015 *Annu. Rev. Condens. Matter Phys.* **6** 383–409
[4] Nandkishore R and Huse D A 2015 *Annu. Rev. Condens. Matter Phys.* **6** 15–38
[5] Alet F and Laflorencie N 2018 *C. R. Physique.* **19** 498–525
[6] Abanin D A, Altman E, Bloch I and Serbyn M 2019 *Rev. Mod. Phys.* **91** 021001
[7] Huse D A, Nandkishore R, Oganesyan V, Pal A and Sondhi S L 2013 *Phys. Rev.* B **88** 014206
[8] Bauer B and Nayak C 2013 *J. Stat. Mech.* **2013** 09005
[9] Kjäll J A, Bardarson J H and Pollmann F 2014 *Phys. Rev. Lett.* **113** 107204
[10] Vosk R and Altman E 2014 *Phys. Rev. Lett.* **112** 217204
[11] Bahri Y, Vosk R, Altman E and Vishwanath A 2015 *Nat. Commun.* **6** 7341
[12] Khemani V, Lazarides A, Moessner R and Sondhi S L 2016 *Phys. Rev. Lett.* **116** 250401
[13] Else D V, Bauer B and Nayak C 2016 *Phys. Rev. Lett.* **117** 090402
[14] Choi S *et al* 2017 *Nature* **543** 221–5
[15] Zhang J *et al* 2017 *Nature* **543** 217–20
[16] Moessner R and Sondhi S L 2017 *Nat. Phys.* **13** 424–8
[17] D'Errico C, Lucioni E, Tanzi L, Gori L, Roux G, McCulloch I P, Giamarchi T, Inguscio M and Modugno G 2014 *Phys. Rev. Lett.* **113** 095301
[18] Schreiber M, Hodgman S S, Bordia P, Lüschen H P, Fischer M H, Vosk R, Altman E, Schneider U and Bloch I 2015 *Science* **349** 842–5
[19] Smith J, Lee A, Richerme P, Neyenhuis B, Hess P W, Hauke P, Heyl M, Huse D A and Monroe C 2016 *Nat. Phys.* **12** 907
[20] Bordia P, Lüschen H P, Hodgman S S, Schreiber M, Bloch I and Schneider U 2016 *Phys. Rev. Lett.* **116** 140401
[21] Choi J Y, Hild S, Zeiher J, Schauß P, Rubio-Abadal A, Yefsah T, Khemani V, Huse D A, Bloch I and Gross C 2016 *Science* **352** 1547–52
[22] Roushan P *et al* 2017 *Science* **358** 1175–9
[23] Bordia P, Lüschen H, Scherg S, Gopalakrishnan S, Knap M, Schneider U and Bloch I 2017 *Phys. Rev.* X **7** 041047
[24] Lüschen H P, Bordia P, Hodgman S S, Schreiber M, Sarkar S, Daley A J, Fischer M H, Altman E, Bloch I and Schneider U 2017 *Phys. Rev.* X **7** 011034
[25] Rubio-Abadal A, Choi J y, Zeiher J, Hollerith S, Rui J, Bloch I and Gross C 2018 arXiv:1805.00056
[26] Basko D M, Aleiner I L and Altshuler B L 2007 *Phys. Rev.* B **76** 052203
[27] Levi E, Heyl M, Lesanovsky I and Garrahan J P 2016 *Phys. Rev. Lett.* **116** 237203
[28] Fischer M H, Maksymenko M and Altman E 2016 *Phys. Rev. Lett.* **116** 160401
[29] Medvedyeva M V, Prosen T c v and Žnidarič M 2016 *Phys. Rev.* B **93** 094205
[30] Monthus C 2017 *J. Stat. Mech.* 043302
[31] Everest B, Lesanovsky I, Garrahan J P and Levi E 2017 *Phys. Rev.* B **95** 024310
[32] Lazarides A and Moessner R 2017 *Phys. Rev.* B **95** 195135
[33] Gopalakrishnan S, Islam K R and Knap M 2017 *Phys. Rev. Lett.* **119** 046601
[34] Breuer H and Petruccione F 2002 *The Theory of Open Quantum Systems* (Oxford: Oxford University Press)
[35] Nandkishore R, Gopalakrishnan S and Huse D A 2014 *Phys. Rev.* B **90** 064203
[36] Johri S, Nandkishore R and Bhatt R N 2015 *Phys. Rev. Lett.* **114** 117401

[37] Nandkishore R 2015 *Phys. Rev.* B **92** 245141
[38] Luitz D J, Huveneers F M C and De Roeck W 2017 *Phys. Rev. Lett.* **119** 150602
[39] Hyatt K, Garrison J R, Potter A C and Bauer B 2017 *Phys. Rev.* B **95** 035132
[40] Lenarčič Z, Altman E and Rosch A 2018 *Phys. Rev. Lett.* **121** 267603
[41] Nandkishore R and Gopalakrishnan S 2017 *Ann. Phys.* **529** 1600181
[42] Žnidarič M, Mendoza-Arenas J J, Clark S R and Goold J 2017 *Ann. Phys.* **529** 1600298
[43] Huse D A, Nandkishore R and Oganesyan V 2014 *Phys. Rev.* B **90** 174202
[44] Ros V, Müller M and Scardicchio A 2015 *Nucl. Phys.* B **891** 420–65
[45] Imbrie J Z 2016 *J. Stat. Phys.* **163** 998–1048
[46] Rademaker L, Ortuño M and Somoza A M 2017 *Ann. Phys.* **529** 1600322
[47] Rademaker L and Ortuño M 2016 *Phys. Rev. Lett.* **116** 010404
[48] Thomson S J and Schiró M 2018 *Phys. Rev.* B **97** 060201
[49] Khemani V, Pollmann F and Sondhi S L 2016 *Phys. Rev. Lett.* **116** 247204
[50] Pollmann F, Khemani V, Cirac J I and Sondhi S L 2016 *Phys. Rev.* B **94** 041116
[51] Wahl T B, Pal A and Simon S H 2017 *Phys. Rev.* X **7** 021018
[52] Kulshreshtha A K, Pal A, Wahl T B and Simon S H 2019 *Phys. Rev. B* **99** 104201
[53] De Tomasi G, Pollmann F and Heyl M 2018 arXiv:1810.04178
[54] Daley A J 2014 *Adv. Phys.* **63** 77–149
[55] Mott N F 1969 *Phil. Mag.* **19** 835–52
[56] Fleishman L and Anderson P W 1980 *Phys. Rev.* B **21** 2366–77
[57] Lee C K, Moix J and Cao J 2015 *J. Chem. Phys.* **142** 164103
[58] Lee C K, Cao J and Gong J 2012 *Phys. Rev.* E **86** 021109
[59] Esposito M and Gaspard P 2003 *Phys. Rev.* E **68** 066112
[60] Hone D W, Ketzmerick R and Kohn W 2009 *Phys. Rev.* E **79** 051129
[61] Thingna J 2013 Steady-state transport properties of anharmonic systems *PhD Thesis* National University Singapore
[62] Vorberg D, Wustmann W, Schomerus H, Ketzmerick R and Eckardt A 2015 *Phys. Rev.* E **92** 062119
[63] Vorberg D, Wustmann W, Ketzmerick R and Eckardt A 2013 *Phys. Rev. Lett.* **111** 240405
[64] Chandran A, Kim I H, Vidal G and Abanin D A 2015 *Phys. Rev.* B **91** 085425
[65] Oganesyan V and Huse D A 2007 *Phys. Rev.* B **75** 155111
[66] Žnidarič M, Prosen T and Prelovšek P 2008 *Phys. Rev.* B **77** 064426
[67] Pal A and Huse D A 2010 *Phys. Rev.* B **82** 174411
[68] Anderson P W 1958 *Phys. Rev.* **109** 1492–505
[69] Gol'dshtein I Y, Molchanov S A and Pastur L A 1977 *Funct. Anal. Appl.* **11** 1–8
[70] Kramer B and MacKinnon A 1993 *Rep. Prog. Phys.* **56** 1469
[71] Žnidarič M, Scardicchio A and Varma V K 2016 *Phys. Rev. Lett.* **117** 040601
[72] Banerjee S and Altman E 2016 *Phys. Rev. Lett.* **116** 116601
[73] Efros A L and Shklovskii B I 1975 *J. Phys. C: Solid State Phys.* **8** L49–51